Predictability of tropical Pacific decadal variability is dominated by oceanic Rossby waves

(Supplementary material)

Xian Wu[1*], Stephen G. Yeager[2], Clara Deser[2], Antonietta Capotondi[3,4], Andrew T. Wittenberg[5], and Michael J. McPhaden[6]

1 Atmospheric and Oceanic Sciences Program, Princeton University, Princeton, NJ

2 National Center for Atmospheric Research, Boulder, CO

3 Cooperative Institute for Research in Environmental Sciences, University of Colorado Boulder, Boulder, CO

4 National Oceanic and Atmospheric Administration /Physical Sciences Laboratory, Boulder, CO

5 National Oceanic and Atmospheric Administration/Geophysical Fluid Dynamics Laboratory, Princeton, NJ

6 National Oceanic and Atmospheric Administration /Pacific Marine Environmental Laboratory, Seattle, WA

Corresponding author: Xian Wu, xw2794@princeton.edu

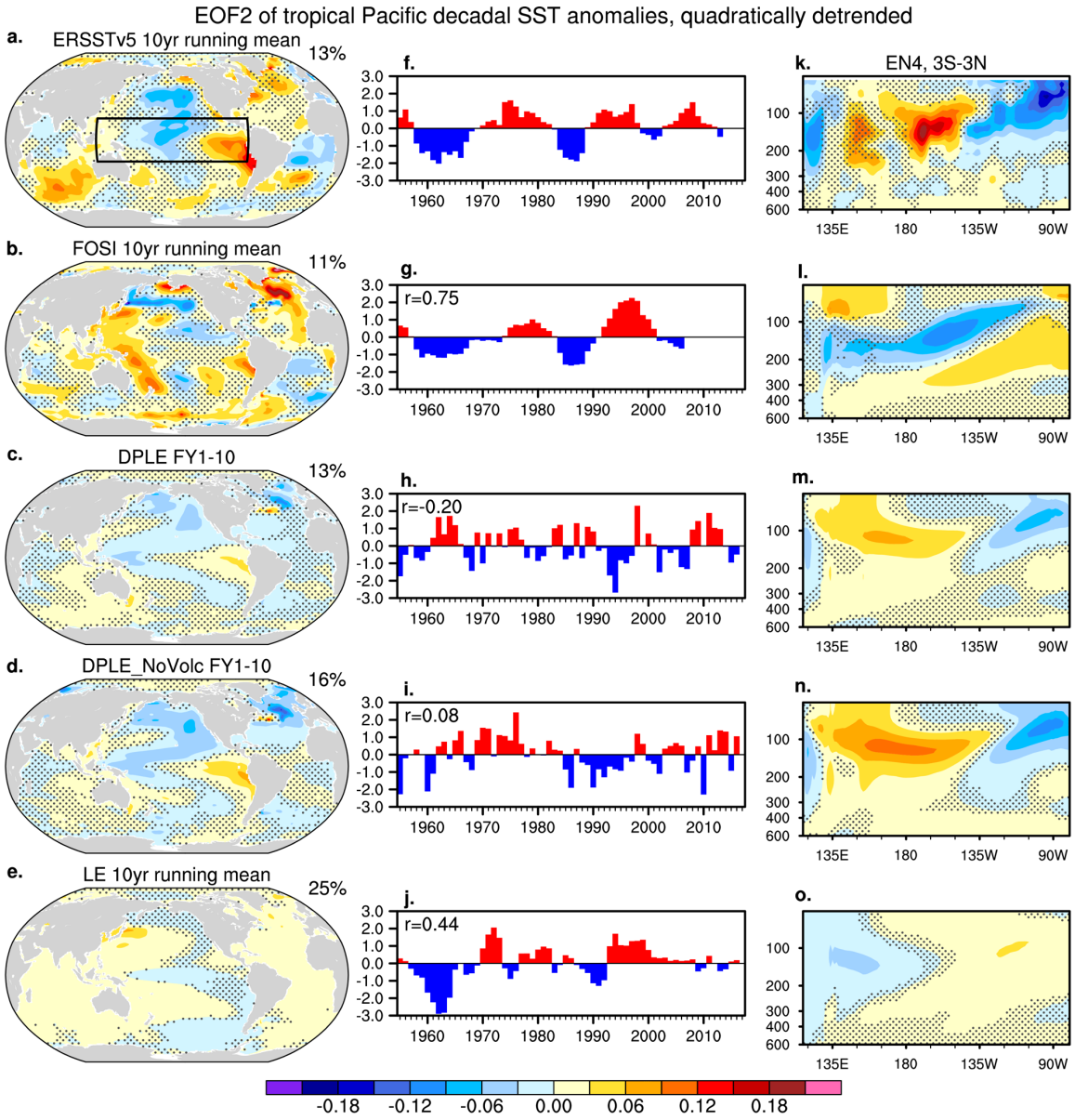

Fig. S1 As in Fig. 1 but for the second leading EOF mode and PC2.

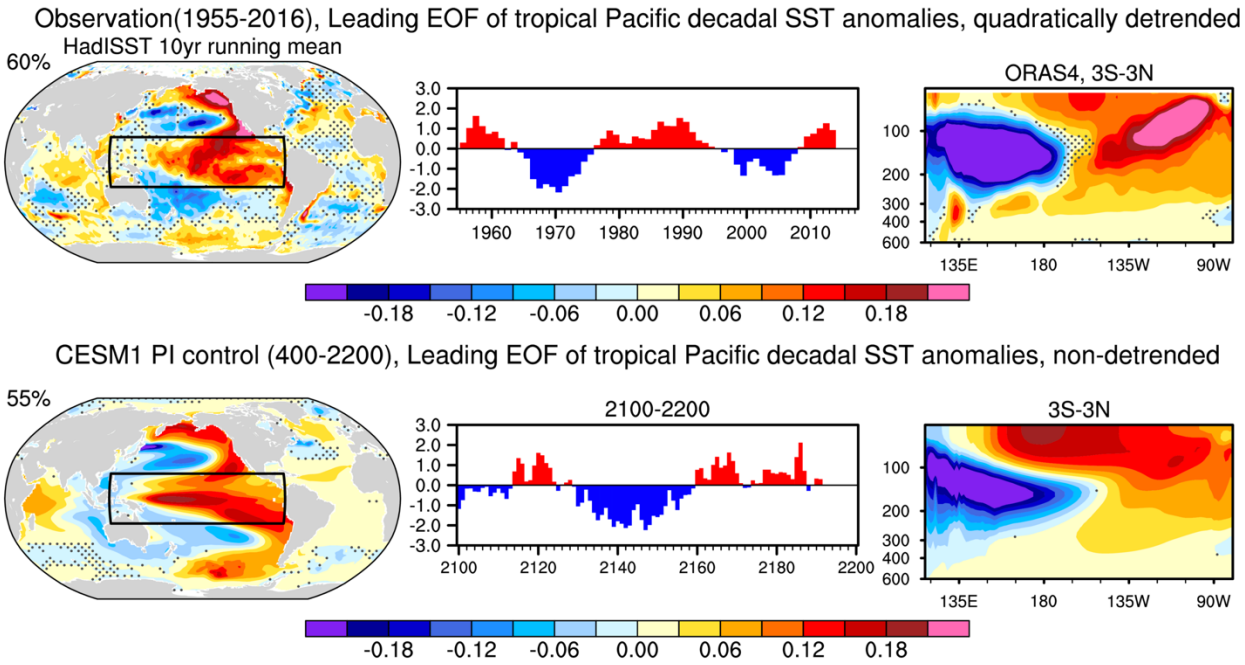

Fig. S2 TPDV simulation in the alternative observational datasets and the CESM1 free-running preindustrial simulation. As in Fig. 1 in the main text, but for (top row) HadISST (1955–2022) and ORAS4 (1958–2019), and (bottom) 1801-yr control simulation of CESM1 under the preindustrial forcing condition. The timeseries of standardized PC1 are only shown for the last 101 years (2100–2200). The year in the axis indicates the start year of any 10-year average window. The numbers in the top-left corner of panels in the first column denote the percentage of total variance explained by the leading EOF mode in each dataset.

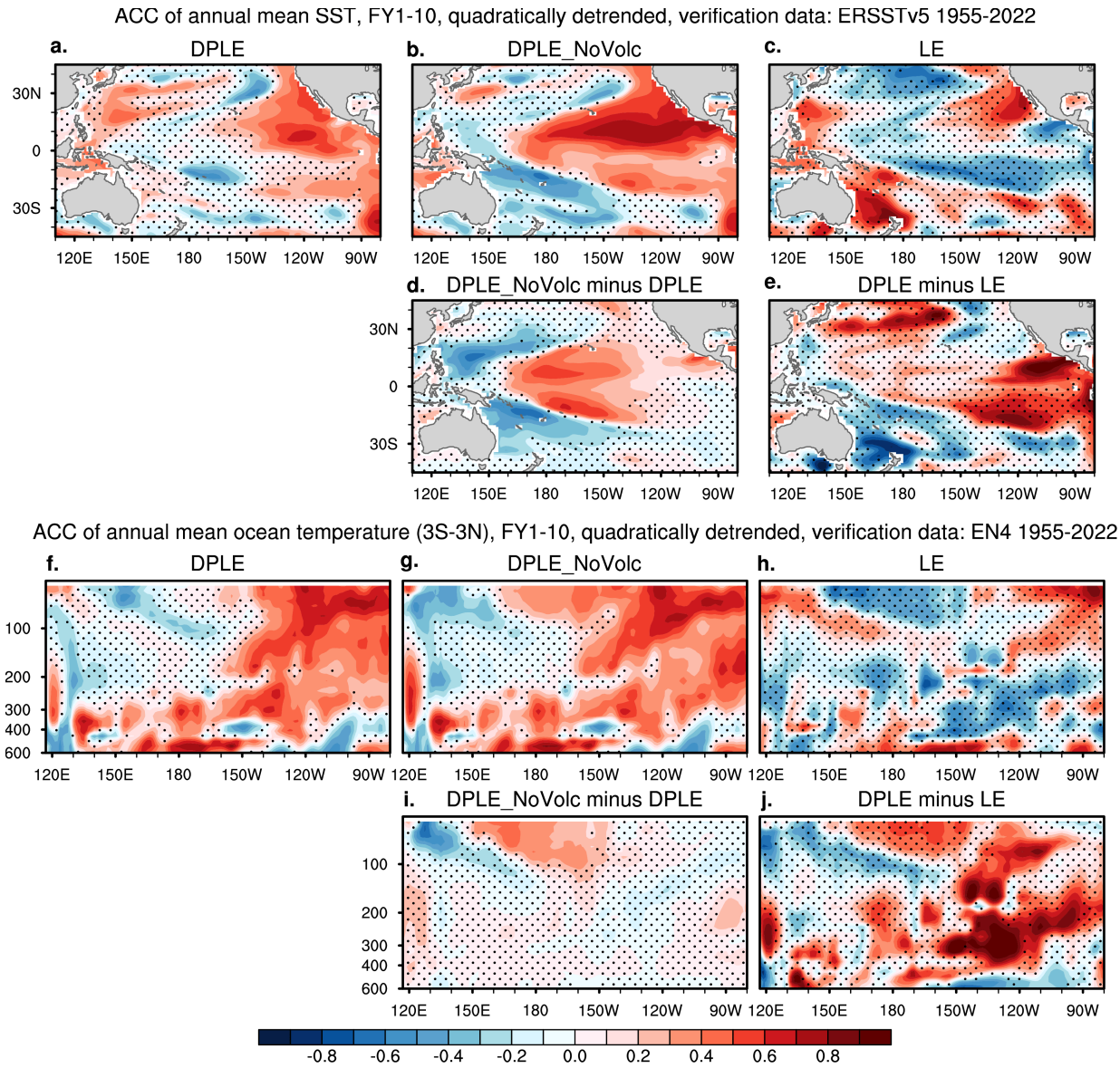

Fig. S3 As in Fig. 2 in the main text, but for skill evaluation relative to observations (SST in ERSSTv5, and ocean temperature in EN4).

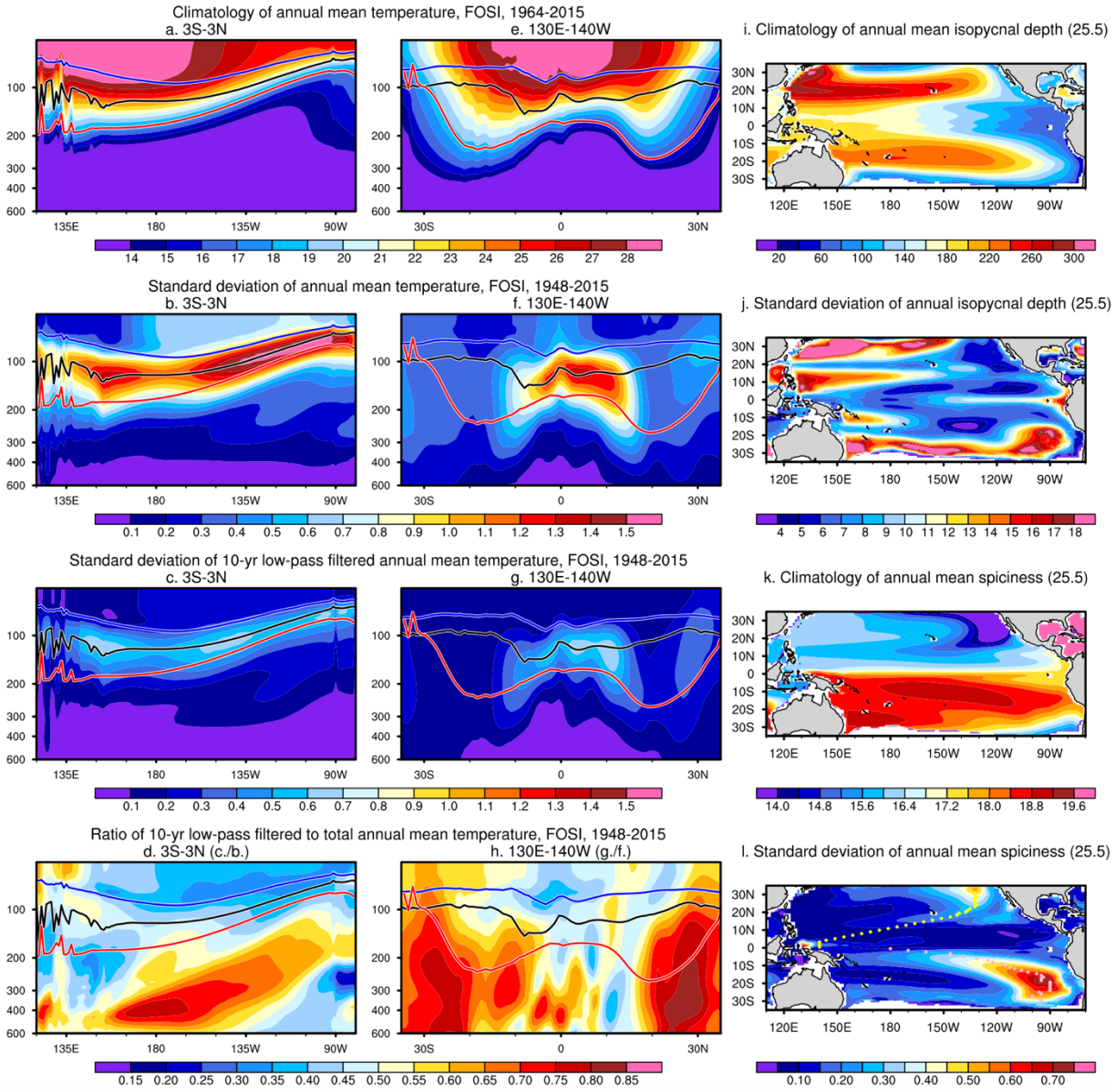

Fig. S4 Definition of different metrics capturing subsurface ocean temperature variability in FOSI. (a) Climatology and (b) standard deviation of equatorial Pacific (3°S–3°N) subsurface ocean temperature, (c) standard deviation of 10-yr low-pass filtered component, and (d) standard deviation ratio of low-pass filtered component of total (non-detrended) annual mean temperature. (e-h) as in a–d but for the zonally averaged (130°E–140°W) subsurface ocean temperature. The curves in a–h denote the climatological mixed layer depth (blue curves), thermocline depth (defined as the depth of maximum vertical temperature gradient; black curves), and isopycnal depth where the potential density is equal to 25.5 kg m^{-3} (σ_{θ}=25.5 kg m^{-3}; red curves). (i) Climatology and (j) standard deviation of annual mean isopycnal depth (σ_{θ}=25.5 kg m^{-3}). (k) Climatology and (l) standard deviation of annual mean spiciness [°C; defined as temperature on the isopycnal depth (σ_{θ}=25.5 kg m^{-3})]. The yellow and pink dots in l denote pathways where spiciness standard deviations are largest at each latitude.

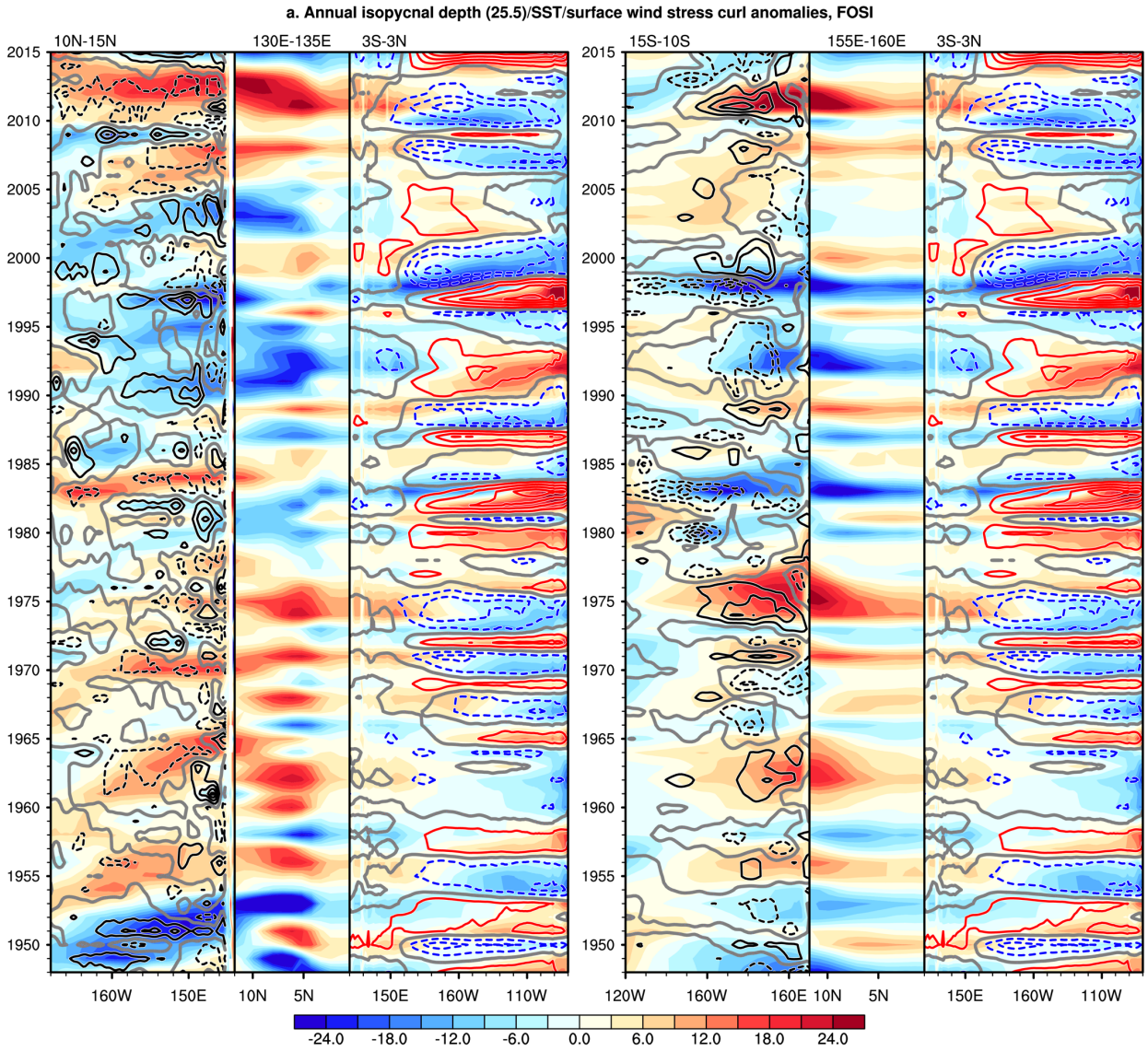

Fig. S5 As in Fig. 3a, but for non-filtered annual mean fields.

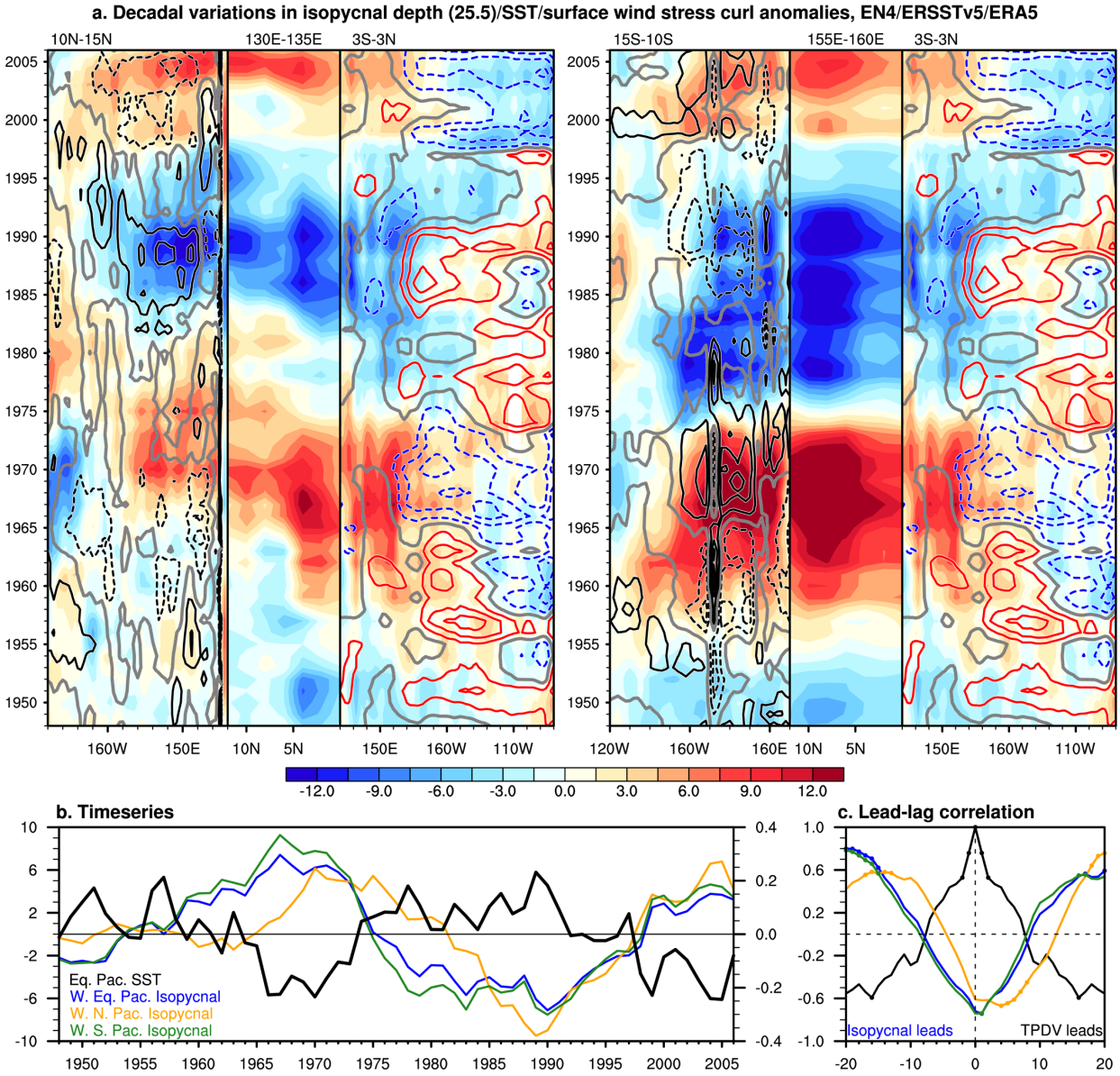

Fig. S6 As in Fig. 3, but using EN4 for isopycnal depth, ERSSTv5 for SST, and ERA5 for surface wind stress curl.

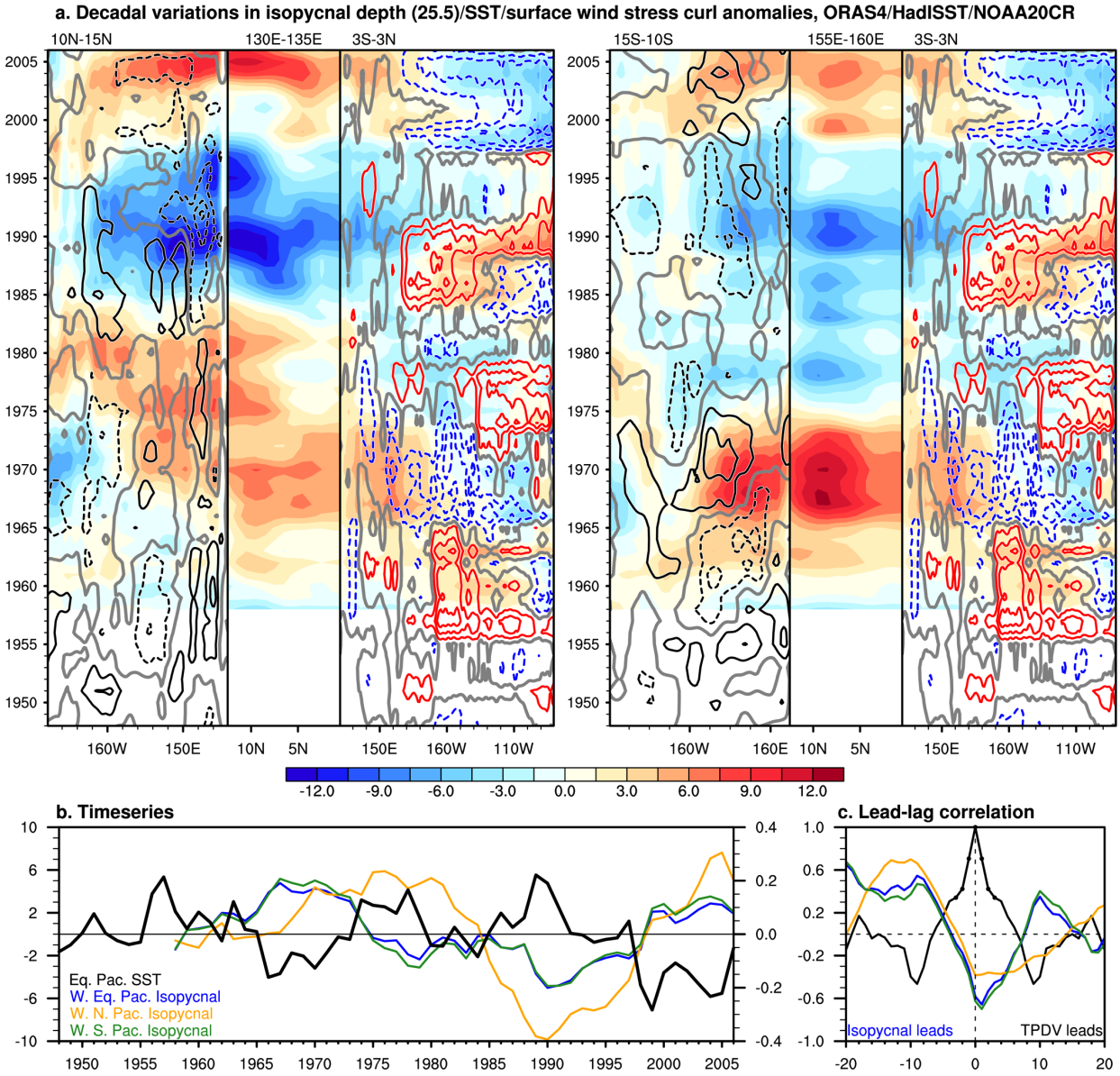

Fig. S7 As in Fig. 3, but using ORAS4 for isopycnal depth, HadISST for SST, and NOAA20CRv3 for surface wind stress curl.

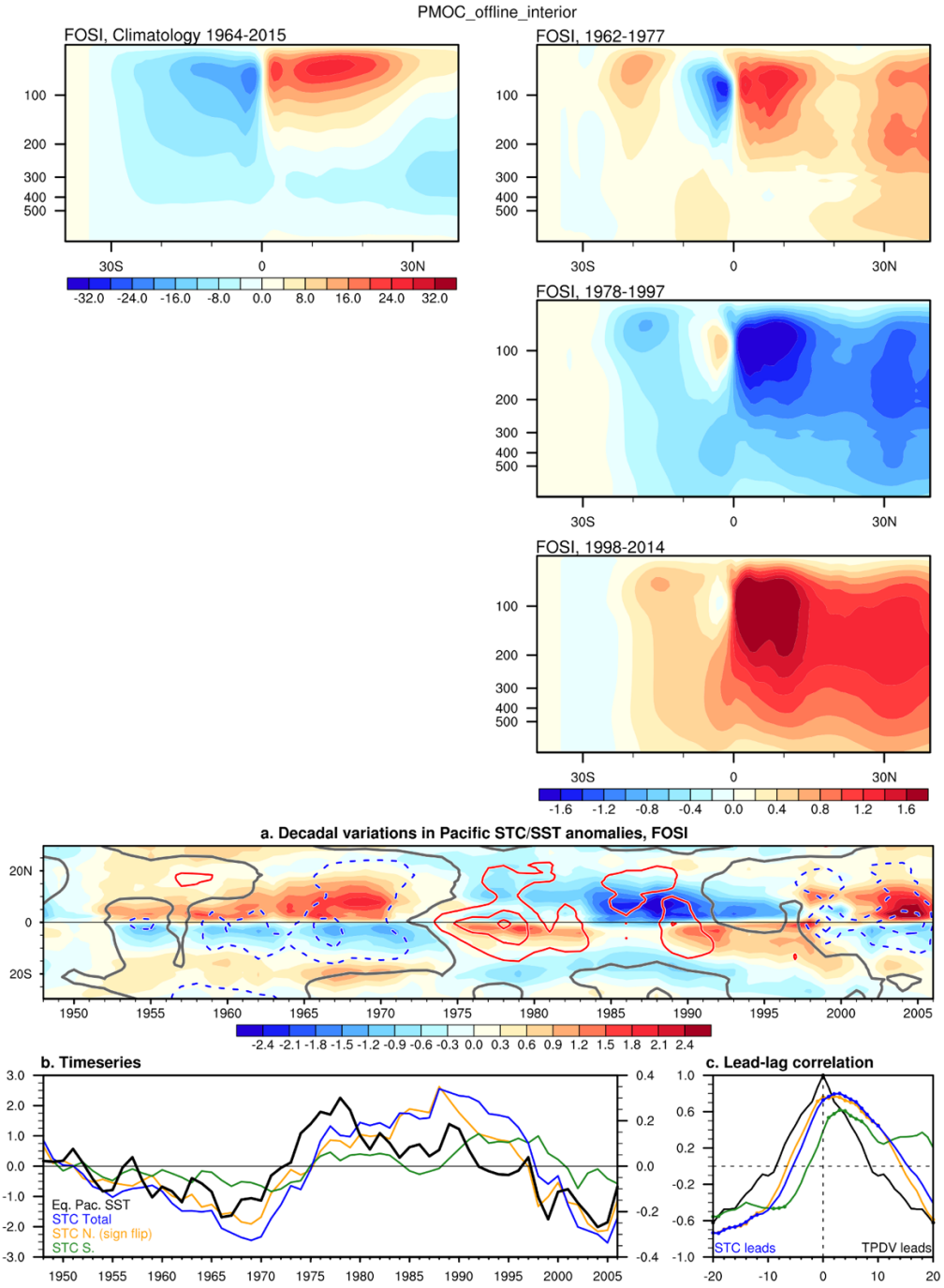

Fig. S8 STC climatology and anomalies associated with TPDV. (top left) Climatology of zonally integrated interior (which excludes the western boundary curents) ocean overturning streamfunction (Sv) as a function of depth (m) and latitude. The zonal integration is taken from the Pacific eastern boundary to 145°E for the Northern Hemisphere and from the eastern boundary to 160°E for the Southern Hemisphere. Postive (negative) values of overturning streamfunction indicate clockwise (anti-clockwise) orbit direction of the transport. (right) Anomalies during the negative TPDV phases (1962–1977; 1998–2014) and positive TPDV phase (1978–1997). (a–c) As in Fig. 4a–c, but based on the total Pacific zonally integrated transport that includes the western boudary currents.

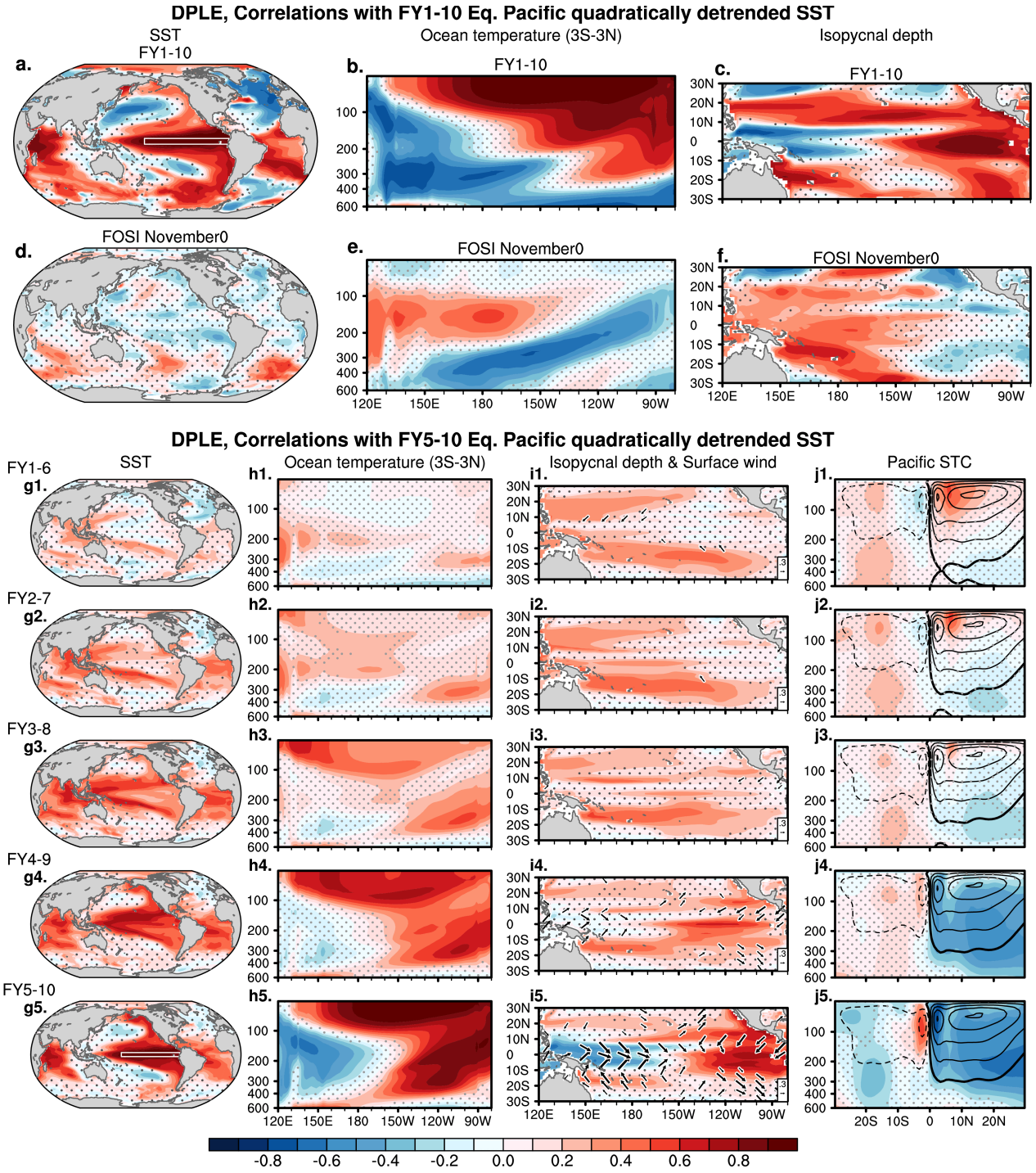

Fig. S9 As in Fig. 5, but for DPLE.

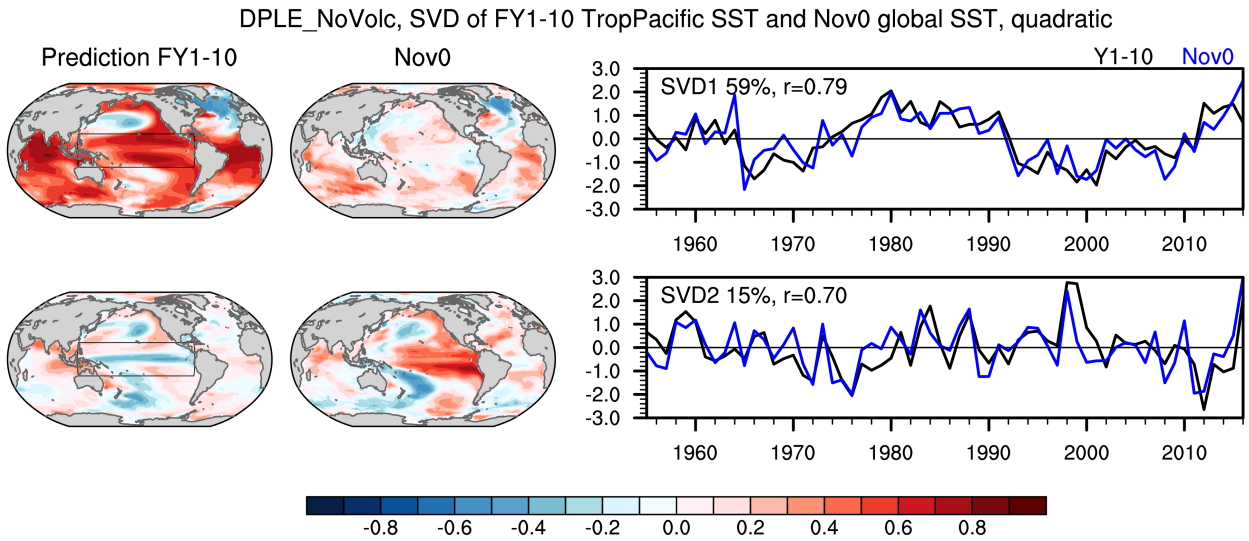

Fig. S10 Pattern and timeseries associated with the (top row) first and (bottom row) second SVD modes of the covariance of predicted tropical Pacific (20°S–20°N, 120°E–120°W) SST anomalies in FY1–10 during 1955–2016, and global initial SST anomalies in Nov0 during 1954–2015. SVD1 explains 59% of the total squared covariance, while SVD2 explains 15%. The expansion coefficients are correlated at a coefficient of 0.79 and 0.70 for SVD1 and SVD2, respectively. (left column) Regression maps of predicted SST at FY1–10 on the standardized Nov0 SST expansion coefficient (blue curve). (middle column) Regression maps of initial SST at Nov0 on the standardized FY1–10 SST expansion coefficient. (right column) Standardized time series of FY1–10 SST (black) and Nov0 SST (blue) expansion coefficients.

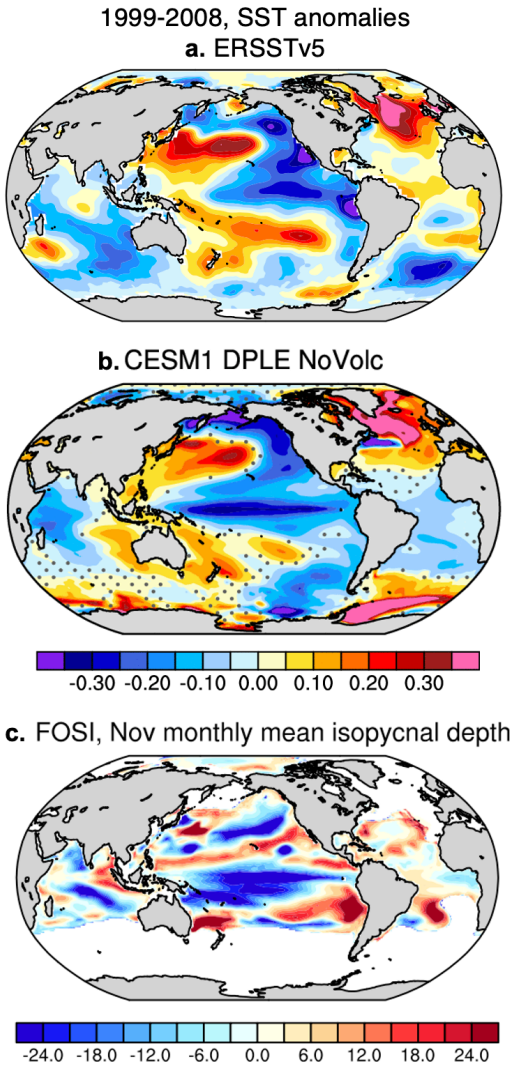

Fig. S11 Quadratically detrended SST anomalies during 1999–2008 in (a) ERSSTv5 and (b) the 10-member ensemble-mean forecast initialized in November 1998 in DPLE_NoVolc using traditional drift correction method (see Methods). (c) Isopycnal depth anomalies (m; σ_{θ}= 25.5 kg m^{-3}) on November 1, 1998, in FOSI.

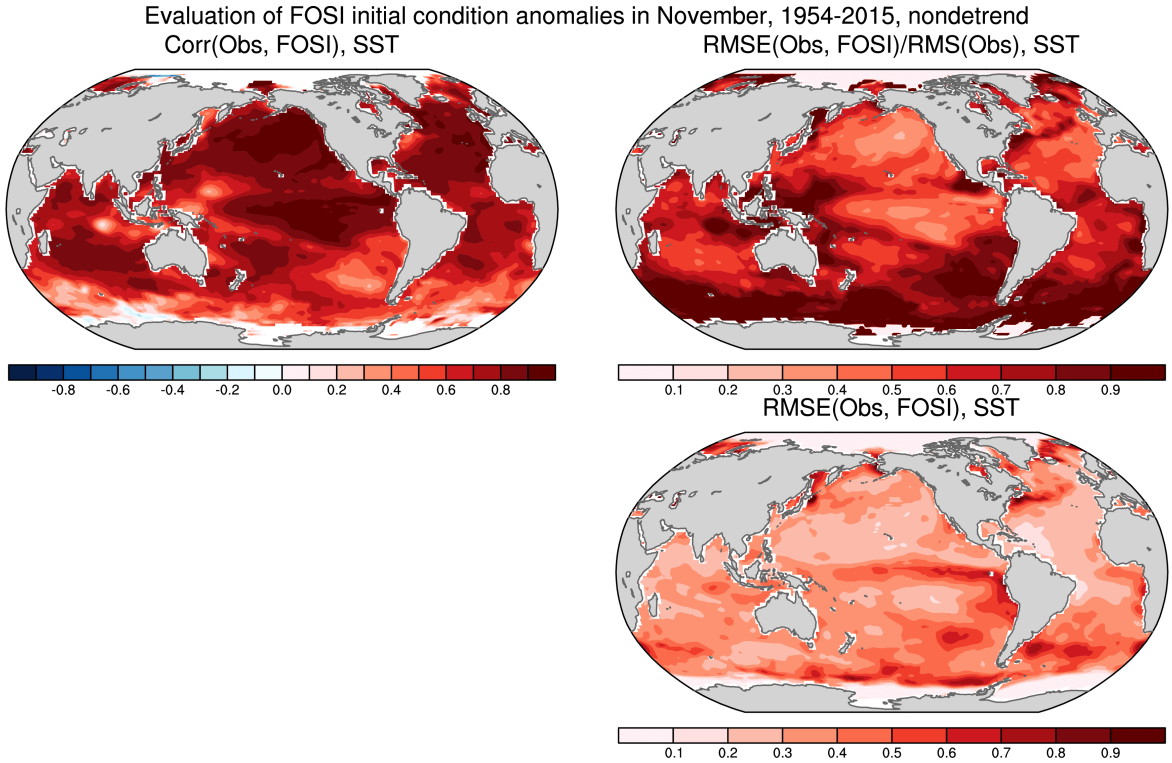

Fig. S12 Evaluation of SST initial conditions in FOSI (top left) Correlation, (top right) standardized Root Mean Square Error (RMSE), and (bottom right) RMSE maps of SST in November in FOSI compared to ERSSTv5 during 1954-2015.

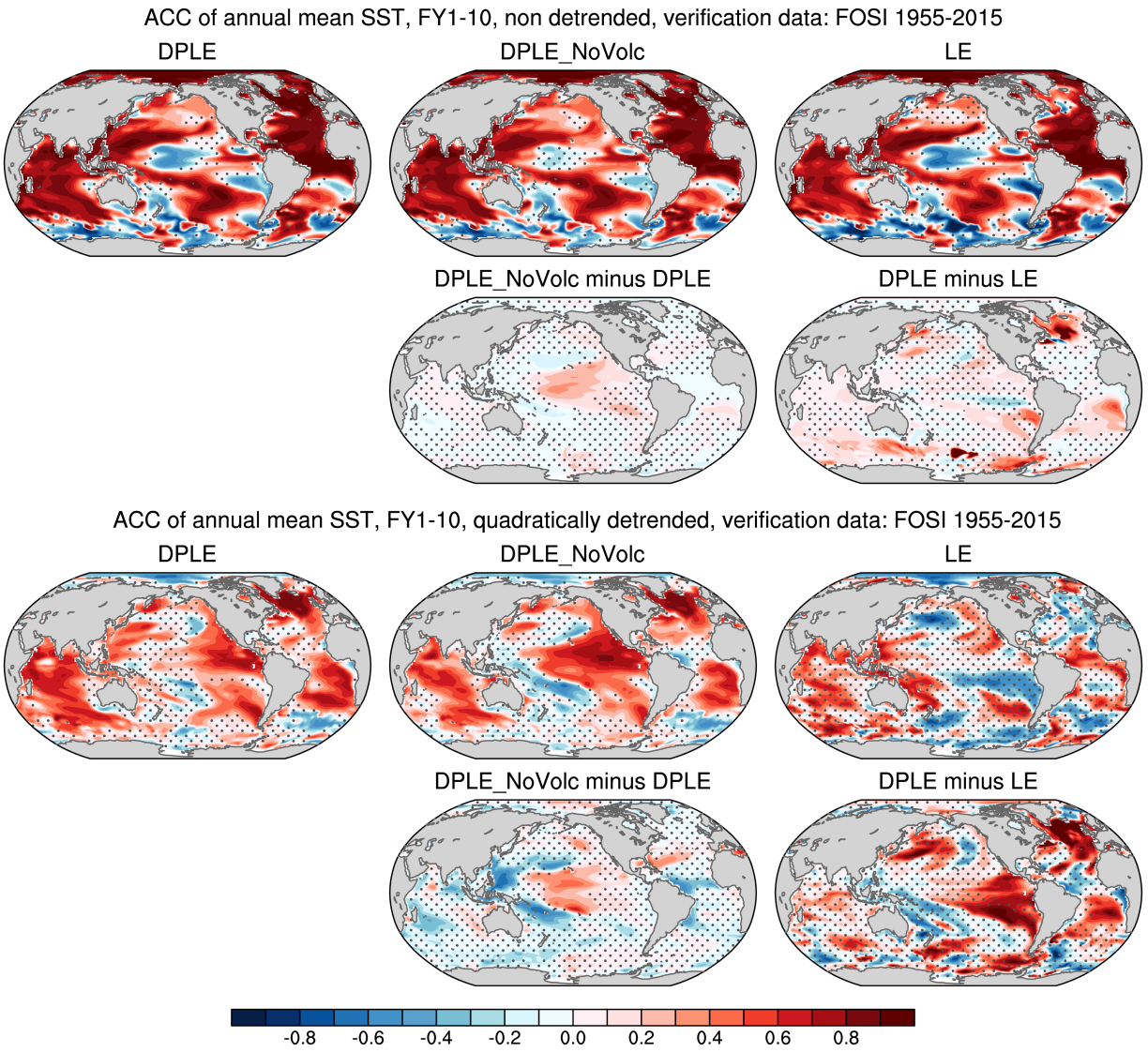

Fig. S13 As in Fig. 2a–e in the main text, but for skill evaluation for the global SST relative to FOSI.

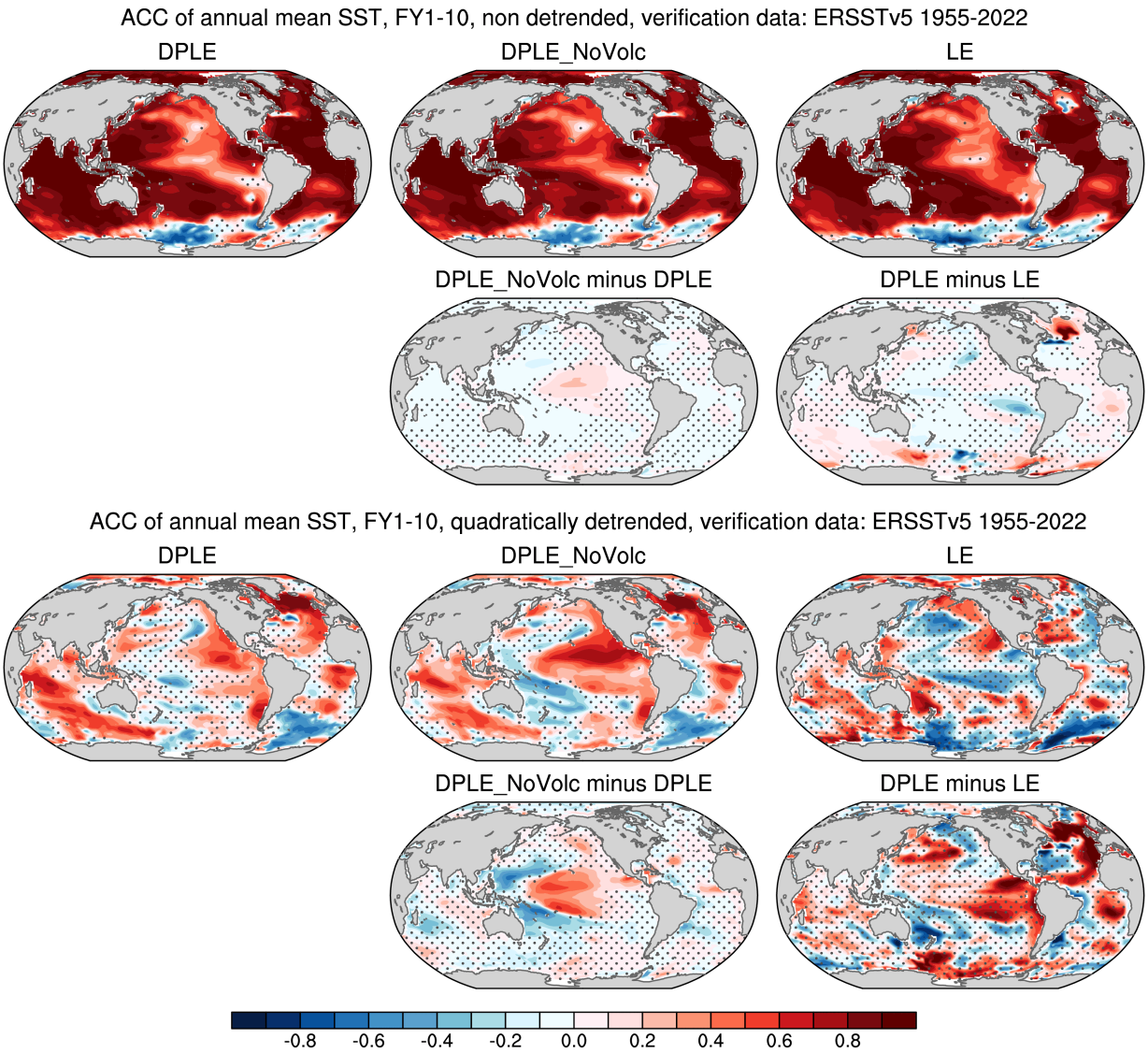

Fig. S14 As in Fig. 2a–e in the main text, but for skill evaluation for the global SST relative to ERSSTv5.